



Measurement of the $t\bar{t}$ Production Cross Section in $p\bar{p}$ Collisions at $\sqrt{s} = 1.96$ TeV Using b -tagged Lepton and Jets Events

The DØ Collaboration
(Dated: August 10, 2004)

A measurement of $t\bar{t}$ production cross section at $\sqrt{s} = 1.96$ TeV, based on the application of lifetime-based b -jet identification techniques to lepton+jets data is presented. Two different tagging algorithms are used. The data sample corresponds to an integrated luminosity of 169 pb^{-1} in e +jets and 158 pb^{-1} in μ +jets channels. The preliminary results yield:

$$\text{CSIP} : \sigma_{t\bar{t}} = 7.2_{-1.2}^{+1.3}(\text{stat})_{-1.4}^{+1.9}(\text{syst}) \pm 0.5 (\text{lumi}) \text{ pb};$$

$$\text{SVT} : \sigma_{t\bar{t}} = 8.2_{-1.3}^{+1.3}(\text{stat})_{-1.6}^{+1.9}(\text{syst}) \pm 0.5 (\text{lumi}) \text{ pb}.$$

Preliminary Results for Summer 2004 Conferences

I. INTRODUCTION

In Run I the Fermilab Tevatron delivered about 100 pb^{-1} of data per experiment, which brought the discovery of the top quark [1]. With the increased statistics and collision energy of Run II the experimental attention turned to precision measurement of top quark properties, in particular its production and decay characteristics. Theoretical predictions performed within the Standard Model predict the production cross section with an uncertainty of less than 15% [2]. Deviations from this rate would signal the presence of new physics, e.g. resonance production of $t\bar{t}$ pairs [3]. In the framework of the Standard Model top quark decays to a W boson and b quark nearly 100% of the time. Top pair production data samples are classified according to W boson decay channels. Data set is referred to as “dilepton”, if both W bosons decay leptonically, “all jets”, if both W bosons decay hadronically and “lepton+jets”, if one of the W bosons decays leptonically and the other one hadronically. The CDF and DØ collaborations previously reported the results of $t\bar{t}$ cross section measurement at $\sqrt{s} = 1.8 \text{ TeV}$ using Run I data sets [4]. CDF collaboration has recently published the first result on top cross section measurement based on Run II data set in dilepton channel [5]. These results are in agreement with the Standard Model predictions, but are statistically limited.

This note reports the result of $t\bar{t}$ cross section measurement in lepton and jets data sample performed using data from Run II of the Tevatron recorded by the upgraded DØ detector. The data sample corresponds to an integrated luminosity of 169 pb^{-1} in e +jets and 158 pb^{-1} in μ +jets channels. The center of mass energy in Run II was increased to $\sqrt{s} = 1.96 \text{ TeV}$, which corresponds to 30% increase in the $t\bar{t}$ production rate. The upgrades of DØ detector allows exploiting long lifetime of b -hadrons to identify b -jets using displaced tracks algorithms, which significantly improve the signal to background ratio in lepton+jets data set.

II. DØ DETECTOR

The DØ Run II detector is comprised of the following main components: the central tracking system, the liquid-argon/uranium calorimeter, and the muon spectrometer.

The central tracking system includes a silicon microstrip tracker (SMT) and a central fiber tracker (CFT), both located in a 2 T superconducting solenoid magnet. The SMT is designed to provide efficient tracking and vertexing capability at pseudorapidities of $|\eta| < 3$. The system has a six-barrel longitudinal structure, each with a set of four layers arranged axially around the beampipe, and interspersed with 16 radial disks. A typical pitch of 50-80 μm of the SMT strips allows a precision determination of the three-dimensional track impact parameter with respect to the primary vertex which is the key component of the lifetime based b -jet tagging algorithms. The CFT has eight coaxial barrels, each supporting two doublets of overlapping scintillating fibers of 0.835 mm diameter, one doublet being parallel to the collision axis, and the other alternating by $\pm 3^\circ$ relative to the axis [6].

The calorimeter is divided into a central section (CC) providing coverage out to $|\eta| \approx 1$, and two end calorimeters (EC) extending coverage to $|\eta| \approx 4$ all housed in separate cryostats. Scintillators placed between the CC and EC provide sampling of showers at $1.1 < |\eta| < 1.4$. [7]

The muon system, covering pseudorapidities of $|\eta| < 2$, resides beyond the calorimetry, and consists of three layers of tracking detectors and scintillating trigger counters. Moving radially outwards, the first layer is placed before the 1.8 T toroid magnets, and the two following layers are located after the magnets. [7]

III. EVENT PRESELECTION

The events under study produce one high P_T lepton, missing energy from an undetected neutrino, two jets from hadronization of b -quarks and two jets from W boson decay. Additional jets are often produced by initial or final state gluon radiation. The event selection starts with the identification of W bosons decaying into a lepton and a neutrino. The signal samples for e +jets and μ +jets channels are preselected requiring, respectively, an electron ($P_T > 20 \text{ GeV}/c$) candidate that satisfies tight quality identification criteria or an isolated muon ($P_T > 20 \text{ GeV}/c$). The missing transverse energy must exceed 20 GeV in e +jets channel and 17 GeV in μ +jets channel. In order to ensure statistical independence from the top cross section measurement in the dilepton channel, events with a second high P_T lepton candidate are discarded. To reduce the contamination of the events with missing energy resulting from lepton energy mismeasurement, we require that the missing energy is not collinear with the lepton direction. W boson candidates can be associated with 1, 2, 3, and 4 or more jets with $E_T > 15 \text{ GeV}$. Signal events are mostly concentrated in the third and fourth jet multiplicity bins, while the first and the second bins, dominated by W boson production in association with jets, are used for a cross check of background normalization. There is still some small contamination from multijet QCD events. The fraction of such events in each jet multiplicity bin is estimated using the so-called Matrix Method [8], which relies on the fact that non- W events have smaller probability to pass tight

TABLE I: Number of events observed after preselection in e +jets and μ +jets samples. Number of W -like and QCD events is estimated using Matrix Method

| | 1jet | 2jets | 3jets | ≥ 4 jets |
|---|-------------------|-------------------|------------------|------------------|
| N_{e+jets}^{presep} | 6452 | 2387 | 595 | 176 |
| $N_{(W \rightarrow e)+jets}^{presep}$ | 6300.5 ± 81.8 | 2268.3 ± 49.7 | 534.8 ± 25.0 | 158.9 ± 13.5 |
| $N_{QCD \rightarrow e+jets}^{presep}$ | 151.5 ± 8.1 | 118.7 ± 4.6 | 60.2 ± 3.1 | 17.1 ± 1.5 |
| $N_{\mu+jets}^{presep}$ | 5134 | 2077 | 510 | 119 |
| $N_{(W \rightarrow \mu)+jets}^{presep}$ | 4933.3 ± 73.9 | 1970.0 ± 46.8 | 473.6 ± 23.2 | 110.5 ± 11.2 |
| $N_{QCD \rightarrow \mu+jets}^{presep}$ | 200.7 ± 10.3 | 106.9 ± 5.7 | 36.4 ± 3.0 | 8.5 ± 1.2 |

lepton quality requirements. Table I summarizes the number of events observed in data and estimated number of QCD and W -like events. At this stage $t\bar{t}$ events are considered as a part of the W -like event subset.

IV. TAGGING ALGORITHMS

Events from $t\bar{t}$ production contain two b -jets, while jets produced in association with W bosons predominantly originate from light quarks or gluons. That is why the signal to background ratio is significantly enhanced after the requirement that at least one of the jets is b -tagged. Among the lifetime based b -tagging algorithms developed by DØ are CSIP and SVT. The simpler of the two - CSIP - relies on counting tracks with significant impact parameter with respect to the primary vertex. If two or more tracks within the jet cone are displaced by more than three standard deviations or three tracks are displaced by more than two sigmas the jet is considered tagged. Tracks are required to have $P_T > 1.5$ GeV/c and to pass a number of quality requirements. The sign of the projection of the impact parameter onto the jet axis can be either positive or negative. Tracks with negative impact parameter are used to quantify the mistagging probability since they originate from misreconstruction/resolution effects while positive tags mainly come from real lifetime effects.

The secondary vertex algorithm (SVT) consists of three main steps: reconstruction and identification of the primary interaction vertex, reconstruction of track-based jets (track-jets), and secondary vertex finding. A calorimeter jet is considered tagged if it contains a selected secondary vertex within the jet cone. Positive (negative) tag is assigned to a jet if a secondary vertex is displaced by more than seven standard deviations from the primary vertex and its transverse decay length is positive (negative).

A. Taggability

Only a jet that satisfies certain requirements on the number and minimum momentum of tracks associated with it can be tagged by either algorithm. These jets are called taggable. The probability for a jet to be taggable, (“the taggability”) depends on event sample and is not fully modelled by Monte Carlo simulation. The concept of taggability is designed to largely decouple the tagging efficiency from issues related to tracking inefficiencies and/or calorimeter noise problems, which are therefore absorbed into the taggability. Taggability was extensively studied and parameterized on data as a function of jet energy and pseudorapidity.

B. Tagging Algorithms Performance

The performance of each algorithm is extensively tested on data. b -tagging efficiency is measured on a dijet data sample for b -jets decaying semi-muonically, and then corrected to reproduce inclusive b -tagging efficiency using the Monte Carlo. The probability to tag a light quark jet (mistag rate) is inferred from the negative tagging rate, corrected for the contribution of the heavy flavor jets to such tags and presence of long lived particles in light quark jets. Both corrections are derived from Monte Carlo. For this analysis the working point of CSIP algorithm is chosen to provide an average mistag rate of 1% per light jet compared to a typical mistag rate of about 0.5% for SVT algorithm. Higher CSIP mistag rate is accompanied by a higher b -tagging efficiency. Therefore in the top cross section measurement SVT and CSIP algorithms complement each other by providing either higher purity of the tagged sample (SVT) or higher efficiency (CSIP).

| | $W+1\text{jet}$ | $W+2\text{jets}$ | $W+3\text{jets}$ | $W+\geq 4\text{jets}$ |
|--------------------------------------|-----------------|------------------|------------------|-----------------------|
| $W+\text{light}$ | 77.2 ± 2.7 | 46.8 ± 1.3 | 15.4 ± 0.7 | 4.4 ± 0.4 |
| $W(c\bar{c})$ | 10.6 ± 0.6 | 6.3 ± 0.2 | 2.08 ± 0.13 | 0.5 ± 0.2 |
| $W(b\bar{b})$ | 25.9 ± 1.1 | 15.6 ± 0.5 | 5.5 ± 0.2 | 1.3 ± 0.3 |
| Wc | 45.9 ± 2.1 | 25.0 ± 0.9 | 6.0 ± 0.3 | 1.10 ± 0.11 |
| $Wc\bar{c}$ | | 6.7 ± 0.5 | 3.0 ± 0.2 | 1.01 ± 0.15 |
| $Wb\bar{b}$ | | 15.4 ± 0.8 | 6.0 ± 0.4 | 2.1 ± 0.2 |
| $W+\text{jets}$ | 159.7 ± 3.6 | 115.7 ± 1.9 | 38.1 ± 0.9 | 10.6 ± 0.6 |
| QCD | 8.5 ± 1.0 | 9.6 ± 1.0 | 4.6 ± 0.7 | 2.0 ± 0.5 |
| single top | 1.38 ± 0.02 | 5.29 ± 0.04 | 2.71 ± 0.03 | 0.97 ± 0.02 |
| $t\bar{t} \rightarrow l\bar{l}$ | 0.80 ± 0.02 | 4.28 ± 0.05 | 2.94 ± 0.04 | 1.00 ± 0.03 |
| VV | 1.21 ± 0.02 | 4.19 ± 0.05 | 0.75 ± 0.02 | 0.09 ± 0.01 |
| $Z \rightarrow \tau^+\tau^-$ | 0.64 ± 0.02 | 0.48 ± 0.03 | 0.26 ± 0.03 | 0.05 ± 0.01 |
| background | 172.1 ± 3.8 | 139.6 ± 2.2 | 49.3 ± 1.2 | 14.7 ± 0.8 |
| syst. | $+11.7-14.4$ | $+8.4-10.2$ | $+3.3-3.4$ | ± 1.3 |
| $t\bar{t} \rightarrow l+\text{jets}$ | 0.14 ± 0.02 | 3.28 ± 0.11 | 15.4 ± 0.2 | 27.8 ± 0.3 |
| total | 172.3 ± 3.8 | 142.9 ± 2.2 | 64.7 ± 1.2 | 42.5 ± 0.8 |
| syst. | $+11.8-14.5$ | $+8.7-10.4$ | $+3.7-4.0$ | $+3.2-5.9$ |
| tagged events in data | 183 | 146 | 74 | 44 |

TABLE II: Summary of observed and predicted number of ℓ +jets events with 1 CSIP tag.

Both b -jet tagging efficiency and the light jet tagging rate are parameterized as functions of jet energy and pseudorapidity. An efficiency to tag a jet containing a c -quark is estimated based on Monte Carlo prediction of b - to c -tagging efficiency ratio. These parameterizations are then used to predict the probability for a jet of a certain flavor to be tagged.

V. BACKGROUND FLAVOR COMPOSITION

We rely on Monte Carlo to predict the flavor composition of the jets produced in association with W boson. The W +jets events with different jet multiplicity and flavor are generated using ALPGEN V1.2 [9] (CTEQ 6.1M) [10] interfaced with PYTHIA 6.2 [11] to simulate hadronization process and underlying event. Events are then processed through the full $D\mathcal{O}$ simulation and reconstruction. The number of tagged W -events is derived based on the number of W -events observed in the data before tagging, multiplied by the fraction of a certain flavor composition and the probability to tag such a combination of jets derived from Monte Carlo calibrated to reproduce data as described above.

The number of tagged QCD events is estimated differently for μ +jets and e +jets samples, because we observe that μ +jets sample has higher heavy flavor fraction compared to a generic multijet sample, while the e +jets sample is essentially identical to the multijet sample in this respect. We use the probability to tag a jet derived from a generic QCD sample to predict the tagging rate in e +jets QCD events. We apply the Matrix Method to the tagged muon sample to predict the amount of non- W events after tagging. In addition to the described background processes there are also small contributions from Z -bosons decaying to τ leptons with one of the τ 's decaying leptonically, Z +jets, diboson and single top production. These backgrounds are estimated based on Monte Carlo simulation.

VI. SAMPLE COMPOSITION AFTER TAGGING

Tables II through V summarize the sample composition after CSIP and SVT tagging algorithms are applied to ℓ +jets events. The $t\bar{t}$ contribution is calculated assuming production cross section of 7 pb. Events that contain exactly one tag and two or more tags are treated separately because they have considerably different signal to background ratio. Figures 1 and 3 show the observed and predicted number of tags for each jet multiplicity. The excess over the background in the third and fourth bins is interpreted as the $t\bar{t}$ signal. Figures 2 and 4 show the number of tagged events in data for each jet multiplicity compared to the background and total Standard Model prediction with the systematic uncertainties.

| | $W+2\text{jets}$ | $W+3\text{jets}$ | $W+\geq 4\text{jets}$ |
|--------------------------------------|------------------|------------------|-----------------------|
| $W+\text{light}$ | 0.18 ± 0.01 | 0.11 ± 0.01 | 0.05 ± 0.01 |
| $W(c\bar{c})$ | 0.04 ± 0.01 | 0.03 ± 0.01 | <0.01 |
| $W(b\bar{b})$ | 0.18 ± 0.01 | 0.12 ± 0.01 | 0.04 ± 0.01 |
| Wc | 0.13 ± 0.01 | 0.07 ± 0.01 | 0.02 ± 0.01 |
| $Wc\bar{c}$ | 0.30 ± 0.02 | 0.16 ± 0.01 | 0.06 ± 0.01 |
| $Wb\bar{b}$ | 3.8 ± 0.2 | 1.47 ± 0.09 | 0.55 ± 0.06 |
| $W+\text{jets}$ | 4.6 ± 0.2 | 1.96 ± 0.09 | 0.72 ± 0.06 |
| single top | 0.73 ± 0.01 | 0.49 ± 0.01 | 0.21 ± 0.01 |
| $t\bar{t} \rightarrow ll$ | 1.14 ± 0.01 | 0.84 ± 0.01 | 0.30 ± 0.01 |
| VV | 0.40 ± 0.01 | 0.08 ± 0.01 | <0.01 |
| $Z \rightarrow \tau^+\tau^-$ | 0.01 ± 0.01 | 0.03 ± 0.01 | <0.01 |
| background | 6.9 ± 0.2 | 3.41 ± 0.09 | 1.24 ± 0.06 |
| syst. | ± 1.0 | ± 0.4 | ± 0.2 |
| $t\bar{t} \rightarrow l+\text{jets}$ | 0.48 ± 0.02 | 4.09 ± 0.06 | 9.47 ± 0.11 |
| total | 7.3 ± 0.2 | 7.50 ± 0.11 | 10.71 ± 0.13 |
| syst. | ± 1.4 | ± 1.4 | $+2.3-2.7$ |
| tagged events in data | 11 | 7 | 8 |

TABLE III: Summary of observed and predicted number of $\ell+\text{jets}$ events with ≥ 2 CSIP tags.

| | $W+1\text{jet}$ | $W+2\text{jets}$ | $W+3\text{jets}$ | $W+\geq 4\text{jets}$ |
|--------------------------------------|-----------------|------------------|------------------|-----------------------|
| $W+\text{light}$ | 34.0 ± 0.5 | 20.6 ± 0.4 | 6.8 ± 0.3 | 1.94 ± 0.17 |
| $W(c\bar{c})$ | 10.1 ± 0.1 | 5.9 ± 0.1 | 1.95 ± 0.08 | 0.43 ± 0.07 |
| $W(b\bar{b})$ | 26.0 ± 0.3 | 15.7 ± 0.3 | 5.6 ± 0.2 | 1.37 ± 0.14 |
| Wc | 43.0 ± 0.5 | 22.7 ± 0.4 | 5.3 ± 0.2 | 0.94 ± 0.08 |
| $Wc\bar{c}$ | | 6.0 ± 0.1 | 2.63 ± 0.10 | 0.94 ± 0.09 |
| $Wb\bar{b}$ | | 15.1 ± 0.3 | 5.7 ± 0.2 | 1.99 ± 0.18 |
| $W+\text{jets}$ | 113.1 ± 0.8 | 86.0 ± 0.7 | 28.0 ± 0.5 | 7.6 ± 0.3 |
| QCD | 7.1 ± 0.9 | 7.6 ± 0.9 | 4.27 ± 0.71 | 1.68 ± 0.41 |
| single top | 1.31 ± 0.02 | 5.1 ± 0.0 | 2.62 ± 0.03 | 0.94 ± 0.02 |
| $t\bar{t} \rightarrow ll$ | 0.75 ± 0.02 | 4.17 ± 0.05 | 2.88 ± 0.04 | 0.98 ± 0.03 |
| VV | 1.11 ± 0.04 | 3.87 ± 0.07 | 0.69 ± 0.03 | 0.08 ± 0.01 |
| $Z \rightarrow \tau^+\tau^-$ | 0.49 ± 0.10 | 0.40 ± 0.10 | 0.21 ± 0.08 | 0.03 ± 0.01 |
| background | 123.9 ± 1.2 | 107.2 ± 1.2 | 38.7 ± 0.9 | 11.3 ± 0.6 |
| syst. | $+12.3-15.0$ | $+8.3-9.8$ | $+2.8-3.1$ | $+0.8-0.8$ |
| $t\bar{t} \rightarrow l+\text{jets}$ | 0.13 ± 0.02 | 3.10 ± 0.10 | 14.9 ± 0.2 | 27.3 ± 0.3 |
| total | 124.0 ± 1.2 | 110.3 ± 1.2 | 53.6 ± 0.9 | 38.7 ± 0.6 |
| syst. | $+12.3-15.0$ | $+8.3-9.7$ | $+3.2-3.4$ | $+3.4-4.8$ |
| tagged events in data | 119 | 120 | 68 | 43 |

TABLE IV: Summary of observed and predicted number of $\ell+\text{jets}$ events with 1 SVT tag.

VII. $t\bar{t}$ PRODUCTION CROSS SECTION

The efficiency to tag $t\bar{t}$ events is estimated using calibrated ALPGEN Monte Carlo similar to estimation of the tagging probabilities for $W+\text{jets}$ events. For $t\bar{t}$ tagging probability turns out to be somewhat higher than for the production of W bosons in association with b -jets because b -jets from top decay are more energetic. The probability to tag a $t\bar{t}$ event with four or more jets is measured to be 61% for CSIP and 58% for SVT.

The cross section is calculated for CSIP and SVT separately by performing a maximum likelihood fit to the observed number of events. Each analysis is considered as 8 different channels: $\mu+\text{jets}$ or $e+\text{jets}$ with 3 or ≥ 4 jets and with one or two or more tagged jets. If the index i refers to a channel ($\mu+3$ jets single tag, $\mu+3$ jets double tag, $\mu+4$ jets single tag or $\mu+4$ jets double tag, $e+3$ jets single tag, $e+3$ jets double tag, $e+4$ jets single tag or $e+4$ jets double tag), then the likelihood \mathcal{L} to observe N_i^{obs} is equal to:

$$\prod_i \mathcal{P}(N_i^{\text{obs}}, N_i^{\text{predicted}}(\sigma_{t\bar{t}})) \quad (1)$$

Here $\mathcal{P}(N^{\text{obs}}, N^{\text{predicted}})$ denotes the Poisson probability to observe N^{obs} events when the prediction is $N^{\text{predicted}}$.

| | $W+2\text{jets}$ | $W+3\text{jets}$ | $W+\geq 4\text{jets}$ |
|---|------------------|------------------|-----------------------|
| $W+\text{light}$ | 0.033 ± 0.001 | 0.021 ± 0.001 | < 0.01 |
| $W(c\bar{c})$ | 0.027 ± 0.002 | 0.017 ± 0.002 | < 0.01 |
| $W(b\bar{b})$ | 0.22 ± 0.02 | 0.14 ± 0.01 | 0.05 ± 0.02 |
| W_c | 0.056 ± 0.002 | 0.027 ± 0.001 | < 0.01 |
| $Wc\bar{c}$ | 0.25 ± 0.01 | 0.12 ± 0.01 | 0.04 ± 0.01 |
| $Wb\bar{b}$ | 3.53 ± 0.08 | 1.32 ± 0.05 | 0.47 ± 0.04 |
| $W+\text{jets}$ | 4.11 ± 0.08 | 1.64 ± 0.06 | 0.58 ± 0.05 |
| single top | 0.65 ± 0.01 | 0.45 ± 0.01 | 0.192 ± 0.005 |
| $t\bar{t} \rightarrow \ell\ell$ | 1.02 ± 0.01 | 0.75 ± 0.01 | 0.27 ± 0.01 |
| VV | 0.39 ± 0.01 | 0.07 ± 0.01 | < 0.01 |
| $Z \rightarrow \tau^+\tau^-$ | 0.04 ± 0.03 | 0.03 ± 0.02 | < 0.01 |
| background | 6.1 ± 0.1 | 2.90 ± 0.10 | 1.00 ± 0.11 |
| syst. | $+1.2-1.1$ | $+0.6-0.5$ | $+0.2-0.2$ |
| $t\bar{t} \rightarrow \ell+\text{jets}$ | 0.40 ± 0.02 | 3.55 ± 0.07 | 8.3 ± 0.1 |
| total | 6.5 ± 0.1 | 6.4 ± 0.1 | 9.3 ± 0.1 |
| syst. | $+1.3-1.1$ | $+1.2-1.1$ | $+2.1-2.2$ |
| tagged events in data | 8 | 8 | 6 |

TABLE V: Summary of observed and predicted number of $\ell+\text{jets}$ events with ≥ 2 SVT tags.

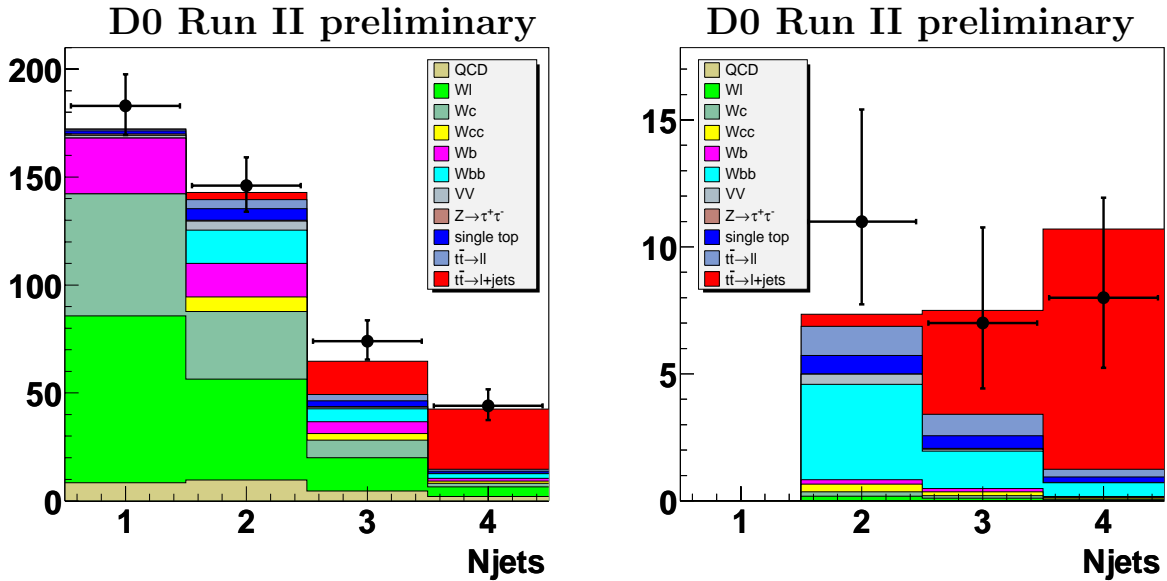


FIG. 1: Summary plot of predicted and observed tagged events in both channels: single CSIP tags (left) and double CSIP tags (right).

The predicted number of events is computed from the background calculations, tagging probabilities as well as the expected number of $t\bar{t} \rightarrow \ell+\text{jets}$ and $t\bar{t} \rightarrow \ell\ell$ events being tagged for a given top quark production cross section. The cross section chosen by the likelihood fit is the one that maximizes the probability of the observed number of events.

The systematic uncertainties on the cross section are obtained for each independent source of uncertainty by varying the source by one standard deviation up and down and propagate the variation into both background estimates and signal efficiencies. A new likelihood function is derived for each such variation to give a new optimal cross section. These variations in the central value of the cross section are then summed quadratically to obtain the total systematic uncertainty.

The $t\bar{t}$ production cross sections measured by the two algorithms are:

$$\text{CSIP} : \sigma_{t\bar{t}} = 7.2_{-1.2}^{+1.3}(\text{stat})_{-1.4}^{+1.9}(\text{syst}) \pm 0.5 (\text{lumi}) \text{ pb};$$

$$\text{SVT} : \sigma_{t\bar{t}} = 8.2_{-1.3}^{+1.3}(\text{stat})_{-1.6}^{+1.9}(\text{syst}) \pm 0.5 (\text{lumi}) \text{ pb}.$$

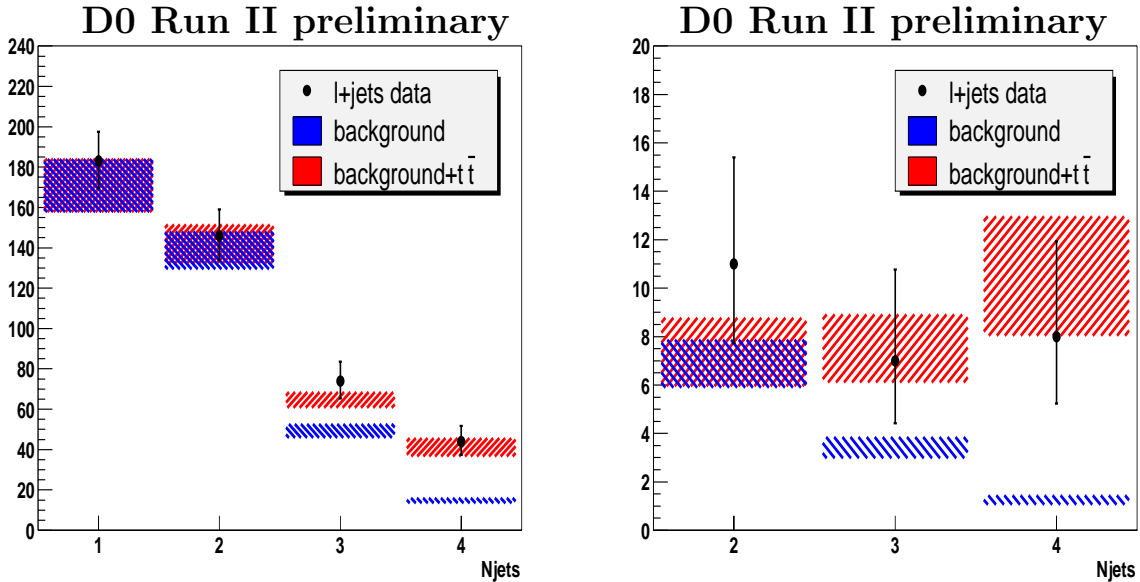


FIG. 2: Summary plot of predicted and observed tagged events in ℓ +jets channel: single CSIP tags (left) and double CSIP tags (right) with systematic uncertainties on signal and background.

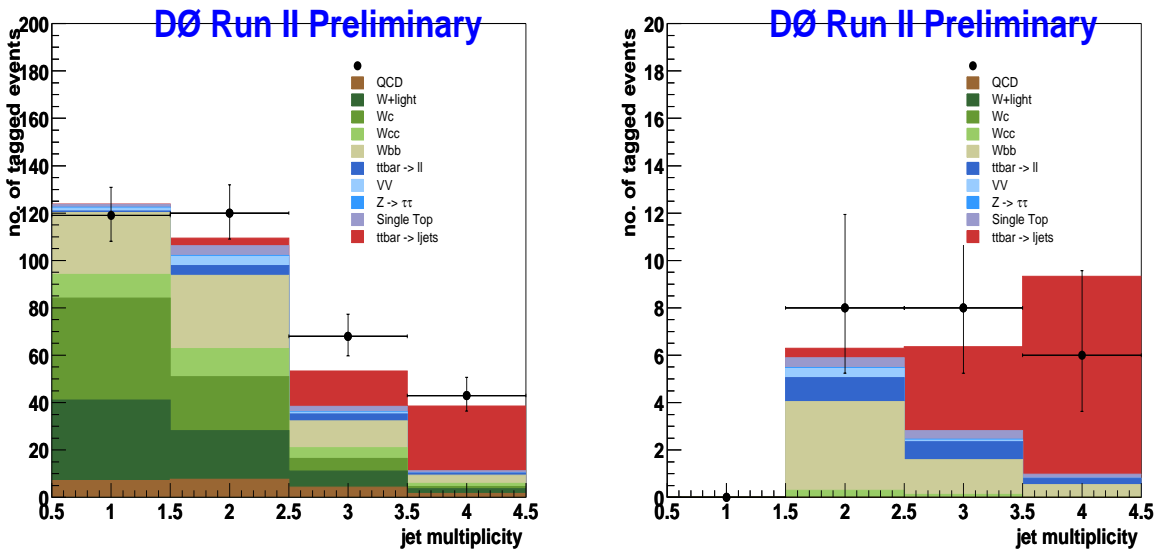


FIG. 3: Summary plot of predicted and observed tagged events in both channels: single SVT tags (left) and double SVT tags (right).

The corresponding likelihood functions ($-2\Delta \ln(\mathcal{L})$) used to obtain the statistical uncertainty on the cross-section are shown in Fig. 5 for CSIP (right) and SVT (left).

VIII. SYSTEMATIC UNCERTAINTIES

The b -jet tagging efficiency measurement in semileptonic decays in data and jet energy scale are the leading sources of systematics in this analysis. Contributions of the main sources of systematic uncertainties into the total error on

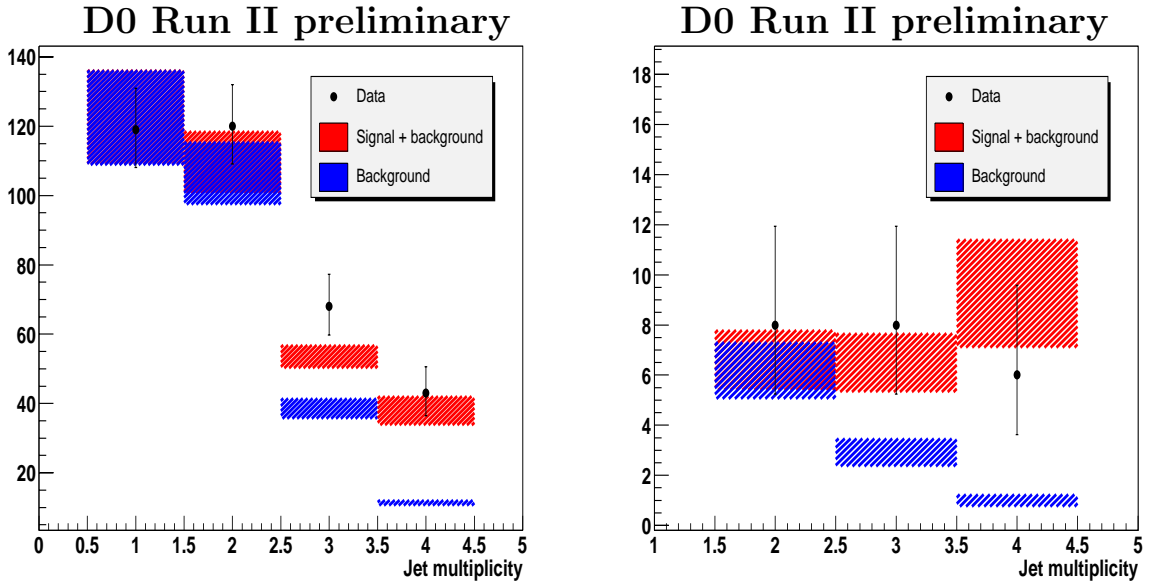


FIG. 4: Summary plot of predicted and observed tagged events in ℓ +jets channel: single SVT tags (left) and double SVT tags (right) with systematic errors on the background and signal.

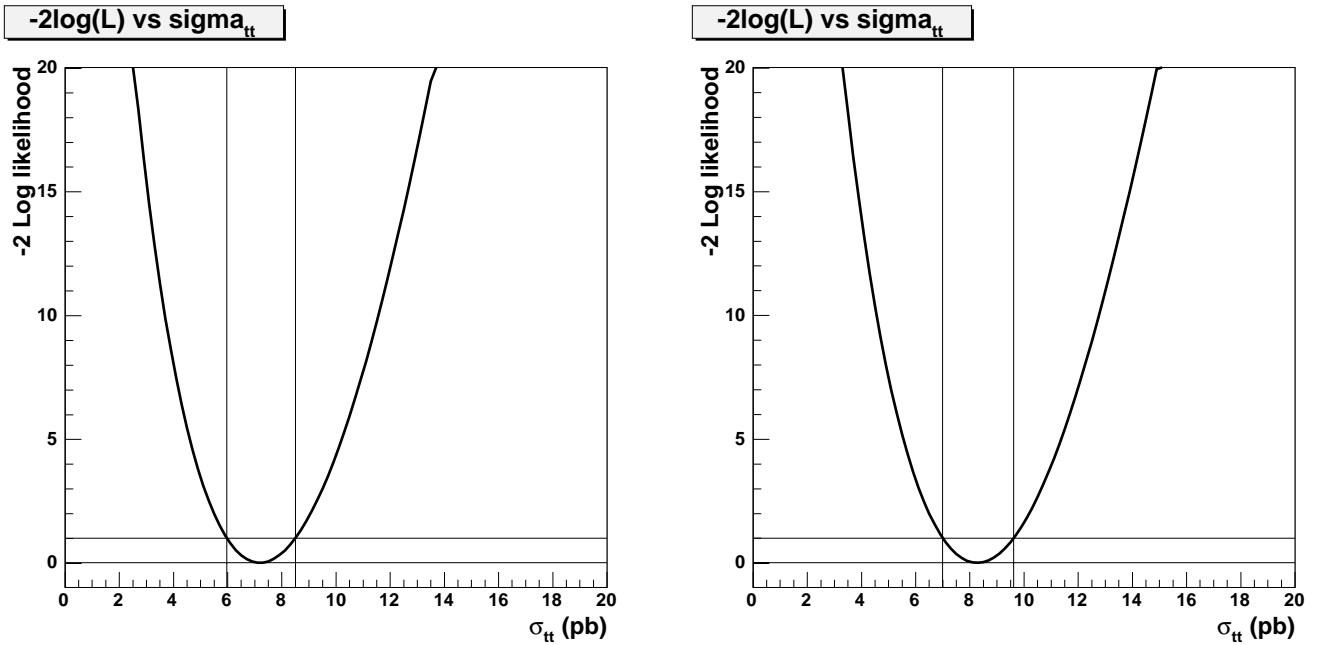


FIG. 5: Likelihood function for CSIP (left) and SVT (right).

the cross section are summarized in Table VI for CSIP and Table VII for SVT.

IX. CONCLUSIONS

The $t\bar{t}$ cross section measurement in lepton and jets data sample is performed using data from Run II of the Tevatron recorded by the upgraded D0 detector. The data sample corresponds to an integrated luminosity of 169 pb^{-1} in

| Source | σ^+ | σ^- |
|--|------------|------------|
| Jet energy scale | 1.01 | -0.59 |
| Jet reco and jet ID | 0.58 | -0.00 |
| Top mass | 0.13 | -0.13 |
| Semileptonic b -tagging efficiency in MC | 0.27 | -0.26 |
| Semileptonic b -tagging efficiency in data | 0.95 | -0.81 |
| b -quark decay model dependence | 0.27 | -0.25 |
| QCD tagging probability | 0.15 | -0.15 |
| $Wb\bar{b}$, $W(bb)$, $Wc\bar{c}$, $W(c\bar{c})$ cross sections | 0.70 | -0.76 |
| Monte Carlo statistics | 0.13 | -0.13 |
| Event statistics for matrix method | 0.18 | -0.17 |

TABLE VI: Breakdown of systematic uncertainties for CSIP for electron and muon channels combined

| Source | σ^+ | σ^- |
|--|------------|------------|
| Jet energy scale | 1.02 | -0.84 |
| Jet reco and jet ID | 0.68 | -0.00 |
| Top mass | 0.24 | -0.23 |
| Semileptonic b -tagging efficiency in MC | 0.41 | -0.44 |
| Semileptonic b -tagging efficiency in data | 0.91 | -0.78 |
| b -quark decay model dependence | 0.34 | -0.32 |
| QCD tagging probability | 0.13 | -0.13 |
| $Wb\bar{b}$, $W(bb)$, $Wc\bar{c}$, $W(c\bar{c})$ cross sections | 0.81 | -0.89 |
| Monte Carlo statistics | 0.08 | -0.08 |
| Event statistics for matrix method | 0.16 | -0.15 |

TABLE VII: Breakdown of systematic uncertainties for SVT for electron and muon channels combined.

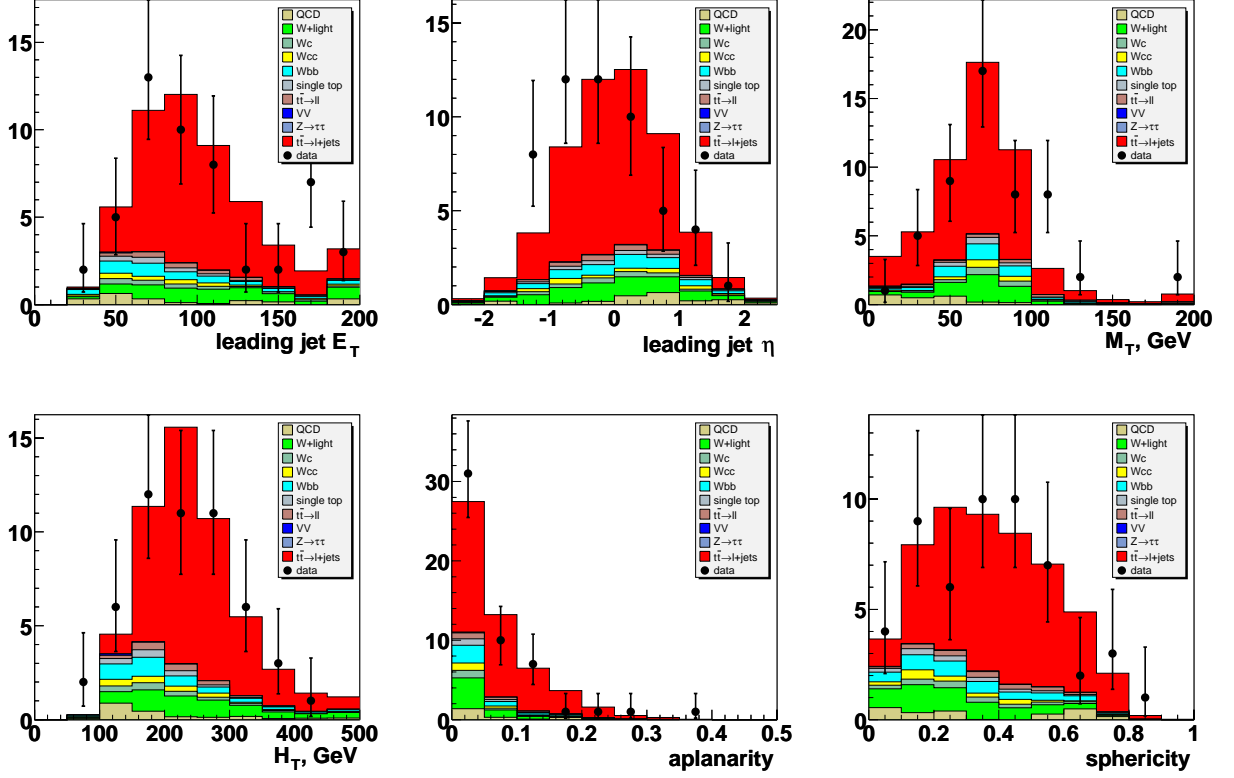
e +jets and 158 pb^{-1} in μ +jets channels. Two different tagging algorithms CSIP and SVT are used to identify b -jets from top quark decay. The results are in a good agreement with each other and with the prediction of the Standard Model.

X. ACKNOWLEDGEMENTS

We thank the staffs at Fermilab and collaborating institutions, and acknowledge support from the Department of Energy and National Science Foundation (USA), Commissariat à l’Energie Atomique and CNRS/Institut National de Physique Nucléaire et de Physique des Particules (France), Ministry of Education and Science, Agency for Atomic Energy and RF President Grants Program (Russia), CAPES, CNPq, FAPERJ, FAPESP and FUNDUNESP (Brazil), Departments of Atomic Energy and Science and Technology (India), Colciencias (Colombia), CONACyT (Mexico), KRF (Korea), CONICET and UBACyT (Argentina), The Foundation for Fundamental Research on Matter (The Netherlands), PPARC (United Kingdom), Ministry of Education (Czech Republic), Natural Sciences and Engineering Research Council and WestGrid Project (Canada), BMBF (Germany), A.P. Sloan Foundation, Civilian Research and Development Foundation, Research Corporation, Texas Advanced Research Program, and the Alexander von Humboldt Foundation.

APPENDIX A: KINEMATIC DISTRIBUTIONS

This section presents a comparison of the kinematic distributions in the fourth jet multiplicity bin of the tagged (≥ 1 tags) $\ell + \text{jets}$ data sample with the ones predicted by a sum of the background and signal contributions obtained from Monte Carlo weighted with the event tagging probabilities for CSIP (Fig. 6) and SVT (Fig. 7). The shapes of all distributions in data are well described by the background and signal contributions, the latter is calculated assuming the $t\bar{t}$ cross section of 7 pb.

FIG. 6: Kinematic distributions for the $\ell + \geq 4$ jets, CSIP.

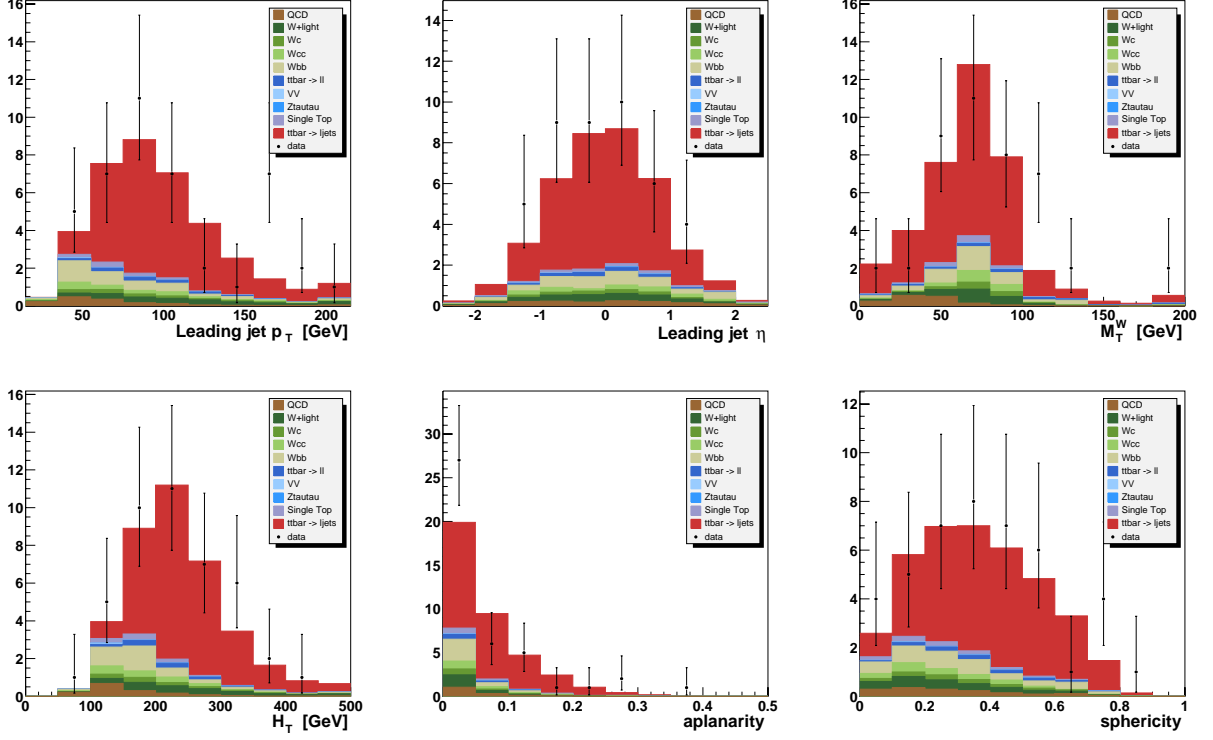


FIG. 7: Kinematic distributions for the $\ell+\geq 4$ jets, SVT.

-
- [1] CDF Collaboration F. Abe *et al.*, Phys. Rev. Lett. **74** 2626 (1995); DØ Collaboration, S. Abachi *et al.*, Phys. Rev. Lett. **74**, 2632 (1995).
- [2] R. Bonciani, S. Catani, M.L.Mangani and P. Nason, Nucl. Phys. B **529**, 424 (1998), updated in arXiv:hep-ph/0303085; N. Kidonakis and R. Vogt, Phys. Rev. D **68**, 114014 (2003).
- [3] C. T. Hill and S.J. Parke, Phys. Rev. D **49**, 4454 (1994); H.P. Nilles, Phys. Rep **110**, 1, (1984); H.E.Haber and G.L. Kane, *ibid.* **117**, 75(1985).
- [4] DØ Collaboration, B. Abbott *et al.*, Phys. Rev. Lett. **79**, 1203 (1997); CDF Collaboration F. Abe *et al.*, Phys. Rev. Lett. **80** 2779 (1998).
- [5] CDF Collaboration D. Acosta *et al.*, FERMILAB-PUB-04/051-E, Resubmitted to Phys. Rev. Lett. May 13, 2004.
- [6] V. Abazov *et al.* (DØ Collaboration), in preparation for submission to Nucl. Instrum. Methods Phys. Res. A; T. LeCompte and H.T. Diehl, "The CDF and DØ Upgrades for RunII", Ann. Rev. Nucl. Part. Sci. **50**, 71 (2000)
- [7] S. Abachi *et al.* (DØ Collaboration), Nucl. Instrum. Methods Phys. Res. A **338**, 185 (1994).
- [8] DØ Collaboration, S. Abachi *et al.*, FERMILAB-Conf-03/200-E.
- [9] M.L.Mangano *et al.*, J. High Energy Phys. **07**, 001 (2003).
- [10] H. L. Lai *et al.*, Eur. Phys. J **C12**, 375 (2000).
- [11] T. Sjostrand *et al.*, Comp. Phys. Commun. **135**, 238 (2001).
- [12] R. Field *et al.*, hep-ex/0404004, Submitted to Phys. Rev. D.